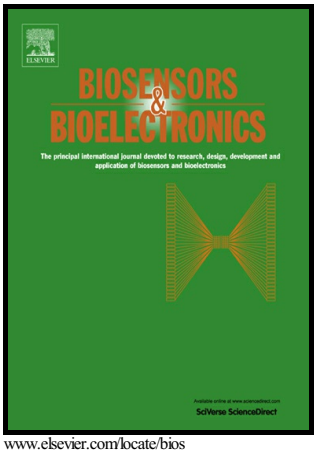

www.elsevier.com/locate/bios

Optoelectronic Fowl Adenovirus Detection Based on Local Electric Field Enhancement on Graphene Quantum Dots and Gold Nanobundle Hybrid

Syed Rahin Ahmed, Jack Mogus, Rohit Chand, Eva Nagy, Suresh Neethirajan

PII: S0956-5663(17)30825-4
DOI: https://doi.org/10.1016/j.bios.2017.12.028
Reference: BIOS10173

To appear in: *Biosensors and Bioelectronic*

Received date: 30 September 2017
Revised date: 15 December 2017
Accepted date: 19 December 2017

Cite this article as: Syed Rahin Ahmed, Jack Mogus, Rohit Chand, Eva Nagy and Suresh Neethirajan, Optoelectronic Fowl Adenovirus Detection Based on Local Electric Field Enhancement on Graphene Quantum Dots and Gold Nanobundle Hybrid, *Biosensors and Bioelectronic,* https://doi.org/10.1016/j.bios.2017.12.028

Optoelectronic Fowl Adenovirus Detection Based on Local Electric Field Enhancement on Graphene Quantum Dots and Gold Nanobundle Hybrid

Syed Rahin Ahmed[1], Jack Mogus[1], Rohit Chand[1], Eva Nagy[2] and Suresh Neethirajan[1*]

[1]BioNano Laboratory, School of Engineering, University of Guelph, Guelph, Ontario, Canada N1G 2W1

[2]Department of Pathobiology, Ontario Veterinary College, University of Guelph, Guelph, Canada

[*]Corresponding author: sneethir@uoguelph.ca (SN)

ABSTRACT

An optoelectronic sensor is a rapid diagnostic tool that allows for an accurate, reliable, field-portable, low-cost device for practical applications. In this study, template-free *In situ* gold nanobundles (Au NBs) were fabricated on an electrode for optoelectronic sensing of fowl adenoviruses (FAdVs). Au NB film was fabricated on carbon electrodes working area using L(+) ascorbic acid, gold chroloauric acid and poly-*l*-lysine (PLL) through modified layer-by-layer (LbL) method. A scanning electron microscopic (SEM) image of the Au NBs revealed a NB-shaped Au structure with many kinks on its surface, which allow local electric field enhancement through light–matter interaction with graphene quantum dots (GQDs). Here, GQDs were synthesized through an autoclave-assisted method. Characterization experiments revealed blue-emissive, well-dispersed GQDs that were 2–3 nm in size with the fluorescence emission peak of

GQDs located at 405 nm. Both Au NBs and GQDs were conjugated with target FAdVs specific antibodies that bring them close to each other with the addition of target FAdVs through antibody–antigen interaction. At close proximity, light–matter interaction between Au NBs and QDs produces a local electric signal enhancement under Ultraviolet–visible (UV-visible) light irradiation that allows the detection of very low concentrations of target virus even in complex biological media. A proposed optoelectronic sensor showed a linear relationship between the target FAdVs and the electric signal up to 10 Plaque forming unit (PFU)/mL with a limit of detection (LOD) of 8.75 PFU/mL. The proposed sensing strategy was 100 times more sensitive than conventional ELISA method.

Keywords: Gold nanobundles; Graphene quantum dots; Optoelectronic biosensor; Fowl adenovirus

1. Introduction

An optoelectronic sensor that reacts to an electrical signal proportional to the incident light is an increasing interest for ultrasensitive, reliable and accurate biosensor development for real-life applications (Bansal et al., 2014). In future, light-to-current transducer technology for diagnostic devices needs to be introduced with surface roughness to create optical confinement in space, which may increase the electric signal and provide a superior detection limit for biosensor. In particular, the biosensing performance is closely related to the interfacial structure of a biosensor that profoundly affects the assembly, binding and signal transduction of biomolecules. The advancement of nanofabrication techniques enables us to refine the surface morphology of biosensor platform, creating needles, pores or different structures on it with the desired

roughness (Ahmed et al., 2012; Ahmed et al., 2014). In particular, plasmonic gold nanostructure is the most attractive material for optical guiding–based biosensors applications because of its stability, easy binding with biomolecules and property of surface plasmon resonance (SPR). In rough plasmonic gold nanostructure, the light travels inside the waveguide, scatters and is confined by total internal reflection that ultimately converts non-radiative light to radiative and enhances the local electric field (Hanke et al., 2012; Kauranen et al., 2012; Oulton et al., Saha et al., 2012; Schuller et al., 2010; Tan et al., 2011; 2008; Yang Tan et al., 2017). This source of light to current conversion enhances the electric signal of the system and enables the development of a highly sensitive optoelectronic sensor for a very low level of detection of target analytes. To date, no optoelectronic biosensor has been reported based on light–matter interactions in plasmonic nanomaterials and semiconductor nanocrystal hybrids to the best of our knowledge. In this study, a nanohybrid of gold nanobundle (Au NB) film and graphene quantum dots (GQDs) was formed through immunoreaction, which offers an exciting route to increase light–matter interaction under UV-visible light irradiation by confining the optical field below the diffraction limit and drives applications in biosensor field.

Nanohybrid materials that allow the combination of two or more nanomaterials in one structure have attracted significant research interest over last few decades and are promising candidates for both academic and practical purposes. In particular, nanohybrids of semiconductor nanocrystal/plasmonic gold films (PGFs) have gained much attention due to: (1) the creation of strong optical confinement through the plasmonic scattering of incident light; (2) the enhanced fluorescence emission due to the amplification of absorbance; and (3) the changing of the nanocrystals fluorescence lifetime because of energy coupling. Those optical modifications in nanohybrids are considered crucial for technological development in the field of nano-optics, and

many research articles have focused on them (Achermann et al., 2010; Cohen-Hoshen et al., 2012; Jiang et al., 2014; Lee et al., 2007; Todisco et al., 2015; Zhang et al., 2013).

However, to date, few articles deal with electric signal enhancement corrected with optical modification in a nanohybrid structure. The light-to-current conversion of nanohybrids is an emerging and exciting frontier, and its popularity has exploded because of novel ways of fabricating plasmonic gold nanostructures with tunable surface roughness. These methods offer unprecedented control of electronic signal modification. In this regard, the light–matter interactions in Au NB/GQD nanohybrid structures that formed through biorecognition phenomena will introduce a new strategy in the optoelectronic nanobiosensor area.

In general, top-down and bottom-up fabrication approaches are suitable to tune the surface morphology of the gold nanostructures. Through top-down approaches such as nanofabrication techniques, a dealloying method gives perfect shape on a metal surface, but this method requires a highly trained personnel and also an expensive technique (Lu et al., 2007; Thiruvengadathan et al., 2013; Yu et al., 2013). In contrast, a bottom-up fabrication of a gold nanostructure using well-known LbL techniques does not require an expert and is cost-effective; hence, the latter is preferable for practical applications (Ariga et al., 2007). Most commonly, gold nanoparticles first are synthesized and then are used to fabricate on a substrate through an LbL process. To reduce the two-step process of the common LbL technique, here we have introduced a single-step *in situ* temple-free gold nanofabrication process on a carbon electrode. For example, PLL and gold salt were deposited on an electrode through an LbL technique in which the top layer was deposited with gold salt; then, at the last stage, ascorbic acid solution was added to reduce the gold salt to a gold nanostructure on the carbon electrode.

The introduction of graphene, a two-dimensional material, enables us to develop various sensing strategies with superior sensitivity due to its unique physical, optical and electrochemical properties. To date, graphene has contributed to electrochemical, optical, photo-electrochemical, piezoelectric and fluorescence sensor development. Among these, the graphene-based fluorescence sensor has attracted a good deal of research interest because of its non-toxicity, optical stability, solubility in aqueous media and environmental friendliness (Sun et al., 2013; Wang et al., 2015, Zheng et al., 2017; Zhou et al., 2016). Over the last few decades, the application of fluorescent materials in bioscience detection systems has occurred reliably and reproducibly. Fluorescent nanomaterials for sensing applications have increased drastically over last few years in preference to organic dye, due to the former's optical stability and aqueous solubility. In particular, cadmium-based fluorescent nanocrystals have gained a good deal of research interest due to their (i) high sensitivity; (ii) specificity in analyte detection; (iii) short time response; (iv) simplicity and (v) cost-effectiveness. Though cadmium-based quantum dots (QDs) are a promising candidate for fluorescence sensing and imaging applications, toxicity to humans and environmental effects are significant concerns, which limits the application of cadmium-based QDs in practical life (Oh et al., 2016; Soenen et al., 2014). Hence, the introduction of real-life-applicable, biocompatible QDs is urgently needed. The discovery of graphene opens the window to create carbon-based, biocompatible graphene QDs (GQDs) with unique optical properties due to quantum confinement effects. Graphene itself lacks fluorescence properties; however, with the size confinement to the nanometer scale, new optical properties can be introduced on it. Until now, different methods of synthesis of GQDs have been reported using both bottom-up and top-down approaches. However, the bottom-up synthesis of QDs is preferable to the top-down approach because the former method allows the QDs to be kept at a

uniform size, which is correlated with the band gap energy of the QDs. Here, we have used bottom-up approaches to synthesize monodispersed and water-soluble, blue-emissive GQDs with the assistance of an autoclave. Furthermore, synthesized GQDs were applied to construct a nanohybrid structure with Au NBs for FAdV detection.

In the present study, fowl adenoviruses (FAdVs), genus of *Aviadenovirus* and a family member of *Adenoviridae*, were chosen as a model analyte that has been associated with a number of diseases in chickens of poultry farms as well as in other birds, causing significant economic losses to the poultry industry. In North America, FAdVs are responsible for several poultry-farm diseases every year: inclusion body hepatitis (IBH), hydropericardium syndrome (HPS), respiratory disease and tenosynovitis (Mittal et al., 2014; Ojkíc et al., 2008).

Currently, FAdV detection techniques involve virus isolation in embryonated eggs and by electron microscopy, the polymerase chain reaction (PCR) technique, the agar gel immunodiffusion (AGID) serological test and enzyme-linked immunosorbent assay (ELISA). Those techniques are time-consuming and laborious. The introduction of time-effective, highly sensitive and specific detection of FAdVs is badly needed to control the spread of diseases in the poultry industries. In the present study, an optoelectronic nanobiosensor was presented for FAdV detection based on electric signal generation related to light–matter interaction in the nanohybrid structure of GQDs/Au NBs.

2. Experimental Section

2.1 Materials and reagents

Gold (III) chloride trihydrate ($HAuCl_4$. $3H_2O$), poly-*l*-lysine (PLL), hydrogen peroxide (H_2O_2), 3,3′,5,5′-tetramethylbenzidine (TMB), Nunc-Immuno 96-well plates, 3-

Mercaptopropionic acid (MPA) and bovine serum albumin (lyophilized powder, ≥96%) were purchased from Sigma-Aldrich (St. Louis, MO, USA). L(+)-ascorbic acid was purchased from Wako Pure Chemical Industries, Ltd (Osaka, Japan). Graphene (Lot No.: GNCP0005) was bought from ACS Material, LLC (Pasadena, CA, USA). Cleaning solution was purchased from Fisher Scientific (Waltham, USA). Immunoassay blocking buffer (Ab 171534, lot: GR 223418-1) was purchased from Abcam, Inc. (Cambridge, UK). Influenza A (H5N2) hemagglutinin antibodies (anti-H5N2 antibodies HA MAb, Lot: HB05AP2609), recombinant influenza virus A (H5N2) HA1 (A/Ostrich/South Africa/A/109/2006)(lot: LC09AP1021) and recombinant influenza virus A (H7N9) HA1 (A/Shanghai/1/2013) (lot: LC09JA2702) were purchased from Sino Biological, Inc. (Beijing, China). Recombinant influenza virus A (H1N1) (California) (CLIHA014-2; lot: 813PH1N1CA) was brought from Cedarlane (Ontario, Canada). Anti-Adenovirus, Group II (HEV) polyclonal antibody was purchased from MyBioSource Inc., San Diego, USA. Chicken whole blood (Cat. No: IR1-080N) was received from Innovation Research, Michigan, USA. The carbon screen-printed electrodes (SPEs) used in this study were made of Dropsens (model C110, Spain). The working area (4 mm diameter) of these SPEs consisted of carbon-paste material, whereas carbon and Ag/AgCl were used to form the counter and reference electrodes, respectively. All experiments were performed using highly pure deionized (DI) water (>18 MΩ·cm).

2.2. Preparation of Au NB film on carbon printed electrode

Au NB film was deposited on carbon printed electrode (working area) through LbL technique with little modification. The working area of carbon electrode was cleaned by a cleaning solution for 30 min, and then thoroughly rinsed with DI water. 10 µL solution of PLL (1 wt %) was

dropped on the working area of the electrode for 10 min. The adsorption area was created with copious amounts of DI water, and it became positively charged at this stage. After that, a negatively charged gold solution (10 µL of $HAuCl_4$, 20 mM) was dropped on it for 10 min at room temperature followed by washing with DI water for several times to remove unbound or loosely bound gold ions. A total of ten (10) bilayers of (PLL/Au ion) were prepared by alternate deposition of PLL and gold solution onto the working area of the carbon electrode. At the upper stage, bilayers of PLL/gold ions were deposited. Finally, 10 µL solution of different concentrations of L(+)-ascorbic acid (0.5, 0.1, 0.05, & 0.01 M) was dropped on the PLL/gold ion layer separately for 30 min, and the color turned pale reddish, which indicates gold nanostructure formation on the working area of the electrode. The electrode was washed with DI water and kept at 4ºC until further use.

2.3. Synthesis of graphene quantum dots (GQDs)

GQDs were synthesized with the assistance of a Benchtop Autoclave (Model: STE-16-C, China). Briefly, 1 mL (0.1 M) of L(+)-ascorbic acid and graphene nanopowder (0.5 mg/mL, 20 mL) were mixed in aqueous media and kept in an autoclave for 1 h at 120°C. The GQD samples were subsequently cooled at room temperature, and the prepared GQD solution was yellow in color, whereas its graphene nanopowder was dark black. Here, L(+)-ascorbic acid acts as a reducing agent, as a stabilizer of QDs.

2.4 Fowl adenovirus-9 (FAdV-9) virus culture

The FAdV-9 strain was cultured to growth in continuous chicken hepatoma cells (CH-SAH cell line) based on a reported previously study (Alexander et al., 1998). The CH-SAH cells were cultivated at 37 ºC with 5% CO_2 in Dulbecco's modified Eagle's medium/nutrient mixture F-12

Ham with 10% non-heat-inactivated fetal bovine serum as previously reported. After infection with the virus, the cells were fed with a maintenance medium of D-MEM/F-12 with all the additions, except that the FBS concentration was reduced to 5%. The FAdV-9 viral titer in allantoic fluid was determined to be 5 $X10^7$ PFU mL^{-1}.

2.5. Specificity of antibodies toward FAdV-9

A conventional enzyme-linked immunosorbent assay (ELISA) method was conducted to check the selectivity of the anti-adenovirus antibody toward FAdV-9. A total of 50 µL (10^4 PFU/mL) of virus solution in a PBS buffer solution (pH 7.5) was added to a PS plate and kept overnight at 4°C. The next day, wells were rinsed three times with PBS buffer solution (pH 7.5), and an immunoassay blocking buffer (Ab 171534, 100 µL) was added and kept at room temperature for 2 h. After washing three times with PBS buffer solution (pH 7.5), anti-FAdV antibody (1 µg/mL), anti-H5N1 NA antibody (1 µg/ml) and anti-H5N2 HA antibody (1 µg/ml) were subsequently added to each of the wells separately and incubated for 1 h. Again, the wells were washed, and horseradish peroxidase–labeled secondary antibody (50 µL, 1 µg/mL) was added and incubated at room temperature for 1 h. Then, unbound or loosely bound secondary antibodies were washed out using PBS buffer (pH 7.5), and TMBZ (10 nM)/H_2O_2 (5 nM) solution was added to each well (50 µL) for 10 min at room temperature. The enzymatic reactions were stopped by adding 10% H_2SO_4 solution (50 µL/well), and the absorbance of the solutions was measured using a microplate reader (Cytation 5, BioTek Instruments Inc., Ontario, Canada) at 450 nm.

2.6 Anti-adenovirus antibody conjugation with Au NBs

FAdV-9 specific antibodies (anti-adenovirus antibody) were bound to Au NBs through amide bonds. Briefly, Au NBs were first functionalized by the addition 10 mM of cysteamine solution for 30 min, and then washed with DI water. The thiol group of cysteamine binds with the gold surface, and the outer layer is covered by the amino group. The addition of 4 mM of EDC, 10 mM of NHS and 1 µL of anti-adenovirus antibodies (5 ng/mL) subsequently on Au NBs overnight at 4ºC helps to bind antibodies with the Au NBs through amide bonds. The binding of antibodies with Au NBs was further confirmed through the conventional ELISA method.

2.7 Binding of anti-adenovirus antibody with GQDs

GQDs were bound with the anti-adenovirus antibody through an electrostatic bond. In brief, positively charged PLL (200 µL, +7.05 eV) was mixed with 800 µL of negatively changed GQDs (-14.07 eV) by gently stirring for 1 h at room temperature. At this stage, GQDs were electrostatically bind with PLL, which is well known for biomolecule immobilization. Here, PLL is used to immobilize the anti-adenovirus (1 µg/mL final concentration of antibody) on its surface. The mixture was then centrifuged (15000 rpm for 30 min) and washed three times with PBS buffer to remove the unbound components.

2.8 Optoelectronic detection of FAdV-9

The developed, antibody-immobilized Au NB film on the electrode was tested for its optoelectronic response under UV-visible light irradiation with respect to varying FAdV concentrations and the addition of antibody conjugated GQDs. At first, the different concentrations of antigen solutions were prepared in PBS buffer (pH 7.4) and chicken blood

samples separately. To perform optoelectronic sensing experiments, at first, 10 µL of various concentrations of FAdV-9 were added to the antibody-conjugated Au NBs for 30 min at room temperature to ensure the antibody–antigen binding. Then, the Au NBs were washed with PBS buffer (pH 7.5) to remove the unbound part. Then, 10 µL of the anti-adenovirus antibody conjugated GQDs were added for 30 min to conjugate with the unbound side of the virus surface through immunoreaction. Then the electrode was washed by gentle immersion in the PBS buffer before analysis of its electrochemical responses with respect to the introduction of a redox probe electrolyte (50 µL of 10 mM $[Fe\ (CN)_6]^{3-}$ + 10 mM $[Fe(CN)_6]^{4-}$ was prepared in 100 mM PBS).

At this stage, Au NBs and GQDs make a hybrid structure at nanoscale proximity through antibody–antigen reaction, and under UV-visible light exposure; light–matter interaction will create strong optical responses that ultimately enhance the electrical signal. The change in the electric signal will be proportional to the presence of the virus concentration. Without the target virus, such a nanohybrid will not be formed, and no changes in current are expected. Blank PBS buffer was used for a baseline correction. The practicability of the proposed assay was further evaluated with chicken blood that represents a complex medium.

2.9 Comparison study of proposed method

The comparison study of the proposed sensing method was conducted with conventional ELISA method. The color developed with different absorbance intensity related to the viral concentration was recorded using a microplate reader. To do so, 50 µL of different concentrated of virus solution in PBS buffer (pH 7.5) was added to polystyrene-coated 96-well plates and kept overnight at 4°C. The wells were rinsed three times with PBS buffer (pH 7.5), and an immunoassay blocking buffer (Ab 171534, 100 µL) was added and kept at room temperature for

2 h. After washing three times with PBS buffer (pH 7.5), anti-adenovirus Ab (1 µg/mL) was added to each of the wells separately and incubated for 1 h. Again, the wells were washed, and horseradish peroxidase–labeled secondary antibody (50 µL, 1 µg/mL) was added and incubated at room temperature for 1 h. Then, unbound or loosely bound secondary antibodies were washed out using PBS buffer (pH 7.5), and TMBZ (10 nM)/H_2O_2 (5 nM) solution was added to each well (50 µL) for 10 min at room temperature. The enzymatic reactions were stopped by adding 10% H_2SO_4 solution (50 µL/well), and the absorbance of the solutions was measured using a microplate reader (Cytation 5, BioTek Instruments Inc., Ontario, Canada) at 450 nm.

2.10 Spectroscopy and structural characterization

Transmission electron microscopy (TEM) images were taken using Tecnai TEM (FEI Tecnai G2 F20, Ontario, Canada). Zetasizer Nano ZS (Malvern Instruments Ltd., Worcestershire, UK) was used for surface charge measurements. Scanning electron microscope images were acquired by Quanta FEG 250 (Oregon, USA). Cyclic voltammograms (CVs) were recorded in the −0.2 to +7 V potential range at a scan rate of 50 mV s^{-1}. The electrochemical measurements were carried out using the mStat 400 potentiostat from DropSens (Spain). Origin Pro 16 (Origin Lab Corporation, MA, USA) was used to draw the graphs. A redox probe solution of 10 mM $[Fe(CN)6]^{3-}$ + 10 mM $[Fe(CN)6]^{4-}$ was prepared in 100 mM PBS (phosphate buffer saline).

3. Results and Discussion

In general, the conjugation of different nanomaterials in a single entity can be achieved in either a direct core-shell synthesis manner or by building a chemical/physical bond between different nanomaterials. At the present study, a two-step approach has been employed to make Au NBs/GQDs nanohybrid through immunoreaction for FAdV detection. At first, Au NBs were

prepared through a modified LbL method on the working area of a carbon electrode and conjugated it with target-specific antibodies through amide bonds. Then, autoclave-assisted nanocrystals of graphene (GQDs) were synthesized and conjugated with target-specific antibodies through electrostatic bond (Scheme 1). Immunoreaction takes place with the addition of FAdVs, and at the same time, Au NBs and GQDs come close to each other to form a nanohybrid structure. The resulting nanohybrids can modify optical properties under UV light exposure through light–matter interaction and enhance electric signal responses in the system (Scheme 1). Without target virus or target-specific antibodies, no possibilities exist to form nanohybrid structures and electric signal enhancement. By changing the virus concentration, we confirmed the creation of an optoelectronic nanobiosensor for FAdVs.

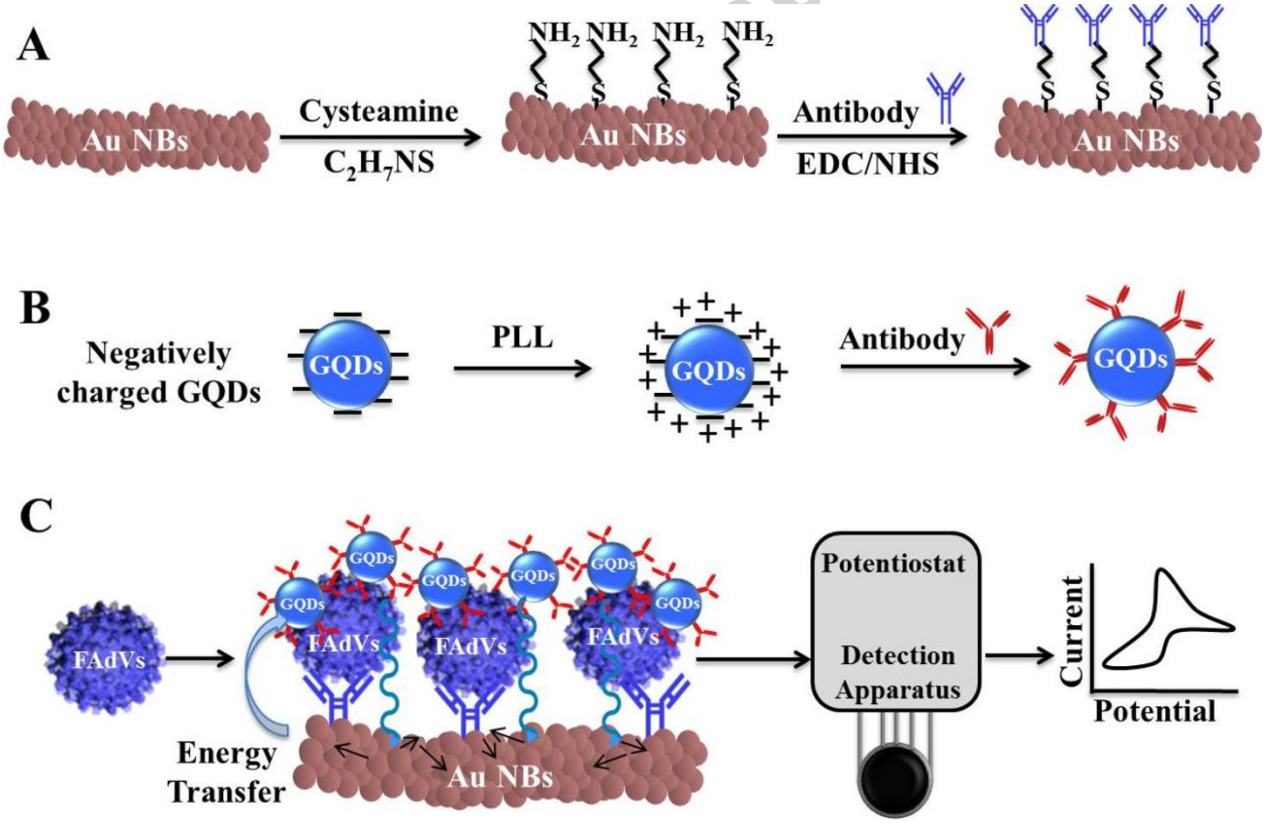

Scheme 1: Schematic presentation of virus sensing: The Au NBs (A) and GQDs (B) were first conjugated with anti-adenovirus antibodies. Then the anti-adenovirus conjugated Au NBs and

GQDs to form a complex (C) in the presence of target FAdVs, finally enhancing the current peak due to light–matter interaction.

3.1. Topographic observation of Au nanostructures

Shape-controlled gold nanostructures were successfully synthesized on a carbon electrode surface by modified LbL techniques without the assistance of any templates. Scanning electron microscopy images of the Au NB film showed the changes of size and shape morphology by varying ascorbic acid concentrations (Fig. 1). Here, Figure 1 A, B C & D represent the Au NB film with ascorbic acid concentrations of 0.5, 0.1, 0.05, & 0.01 M respectively. The initial surface morphology of Au nanostructure with ascorbic acid concentration 0.5M was a cauliflower-like shape (Fig 1A), which turned into a flower-like shape when the ascorbic acid concentration was decreased to 0.1 M (Fig. 1B). It is clear that few arms were produced on the Au nanostructure with decreasing concentrations of reducing agents. At an ascorbic acid concentration of 0.05 M, a dendrite-shaped Au nanostructure was formed with many arms and branches and extended all the way from the center of the particles (Fig. 1C). The length and diameter of the branches were ≈1.2 μM and ≈20 nm respectively. An Au nanostructure with a bundle-like shape was formed on the electrode with a reducing agent concentration of 0.01M (Fig. 1D). A close-up view of the surface of Au NBs reveals a surface morphology formation of grain-like nanostructures (length and diameter were ≈700 nM and ≈10 nm respectively) that makes the surface roughen with many kinks and terraces. With decreasing reducing agent concentrations, the surface morphology of gold nanostructures tended to grow more complicated. Such complex surface structures possess higher biomolecule capture efficiency that greatly influences the detection limit of the biosensor. It is well known that the concentration of the

reducing agent determined the size and shape of nanoparticles (NPs). At lower concentrations, due to inability to reduce Au^{3+} to Au NPs, larger, non-spherical shapes usually formed. Here, the NPs shape is fully determined thermodynamically by surface-free energies whose order is (111) < (100) < (110). Here, the low surface-free energy facets such as {111} or {100} are actively dominant to form non-spherical-shaped NPs (Ahmed et al., 2017). In this study, Au NB shapes were formed on a carbon electrode with a lower concentration of reducing agent. The Au NBs' surface morphology contains many kinks and terraces for incident light scattering and confinement and converts non-radiative light to radiative (Fig. 1 D). Those phenomena enable the creation of a strong coupling regime and could be potential candidates for bioanalytical assay applications.

Figure S1 shows the UV-visible spectra of Au NBs formed on the carbon electrode (working area) from the different concentrations of L-(+)-ascorbic acid. The absorbance of different Au NBs shows a broader spectrum with decreasing reducing agent concentration due to the formation of anisotropic-shaped nanostructures and plasmon resonance splitting effects on the nanostructures.

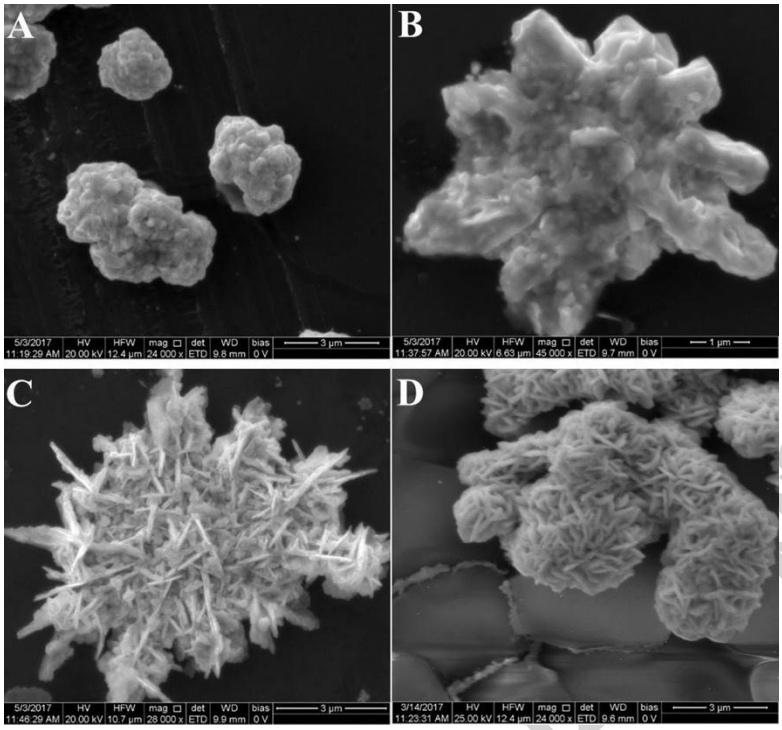

Figure 1: SEM images of Au nanostructures formed on a carbon electrode with different concentrations of L-(+)-ascorbic acid: (A) 0.5, (B) 0.1, (C) 0.05 and (D) 0.01 M.

To conduct an optoelectronic bioassay, the concentration of L (+)-ascorbic acid was selected at 0.01 M to form Au NBs on the working area of the electrode (Fig. 2A). An SEM image of Au NBs shows NBs were formed over a large area of the electrode whereas a close SEM image confirmed the bundle shapes of Au nanostructure (Fig. 2 B&C). Furthermore, the elementary analysis of the Au NB film revealed that the NB area was full of gold elements, whereas other parts of the electrode (the unfabricated part) had no sign of gold metal (Fig. 2D).

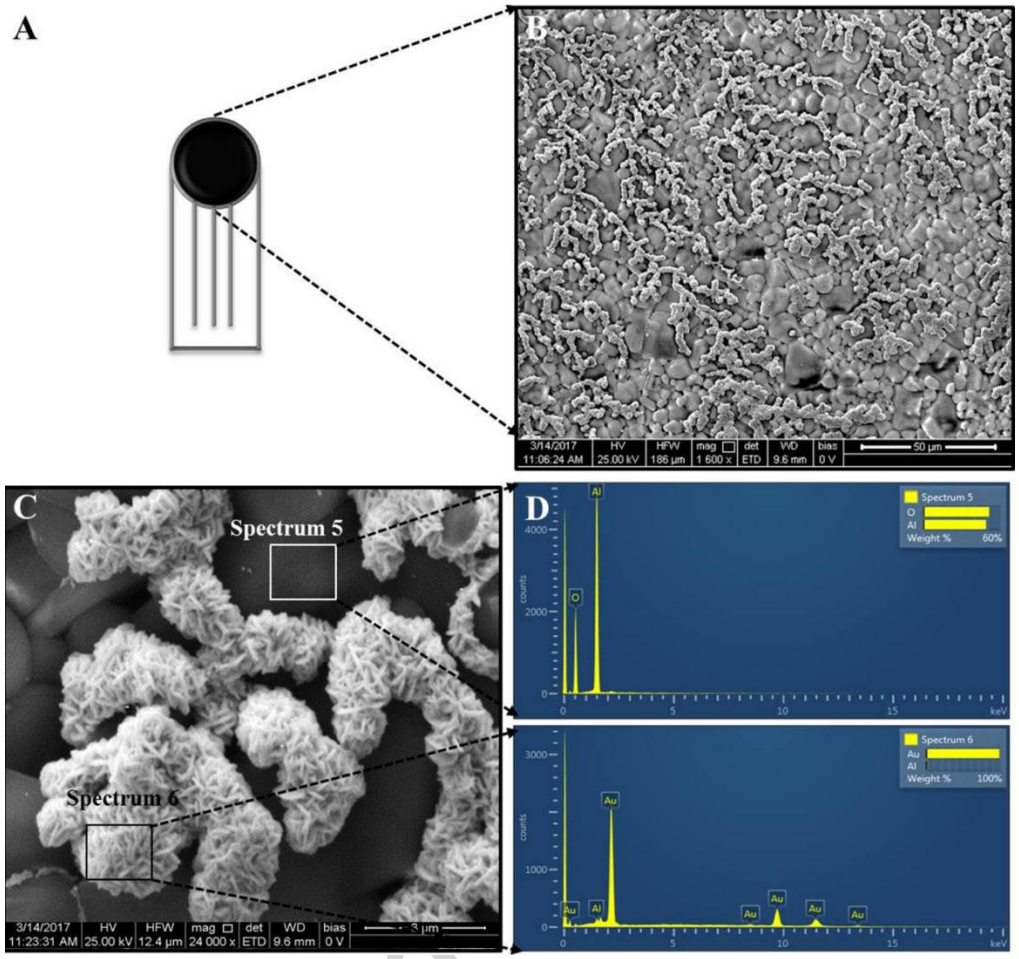

Figure 2: (A) Fabrication of Au NBs on the working area of a carbon electrode; (B) SEM images of Au NBs formed on the carbon electrode with an L-(+)-ascorbic acid concentration of 0.01 M; (C) Close view of Au NBs & (D) Elementary analysis profile of Au NBs.

3.2. Characterization of GQDs

The photoluminescence intensity and UV-vis spectrum of GQDs were located at 405 nm and 350 nm respectively, as shown in Figure 3A. Synthesized GQDs exhibited a yellow color to the naked eye, whereas under UV-light, a strong blue color was apparent (Fig. 3B).

The quantum yield (QY) of synthesized GQDs was determined using Rhodamine 6G dissolved in ethanol as a reference standard (Φ_F=0.95). The following Equation (1) was used to calculate QY:

$$\Phi_F = \Phi_{F(Std)} \frac{F.A_{Std}.n^2}{F_{Std}.A.n^2_{Std}} \quad (1)$$

In the above equation, Φ_F represents the PL QY of the GQDs, $\Phi_{F(Std)}$ represents the PL of the standard, F and F_{Std} denote the integrated sums of the PL intensity of the GQDs and standard respectively, A and A_{Std} signify the optical densities of the GQDs and the standard respectively, and n^2 and n^2_{Std} represent the refractive indexes of the solvents used to dissolve the QDs and the standard respectively. The corresponding PL QY value of the GQDs was 11.26%.

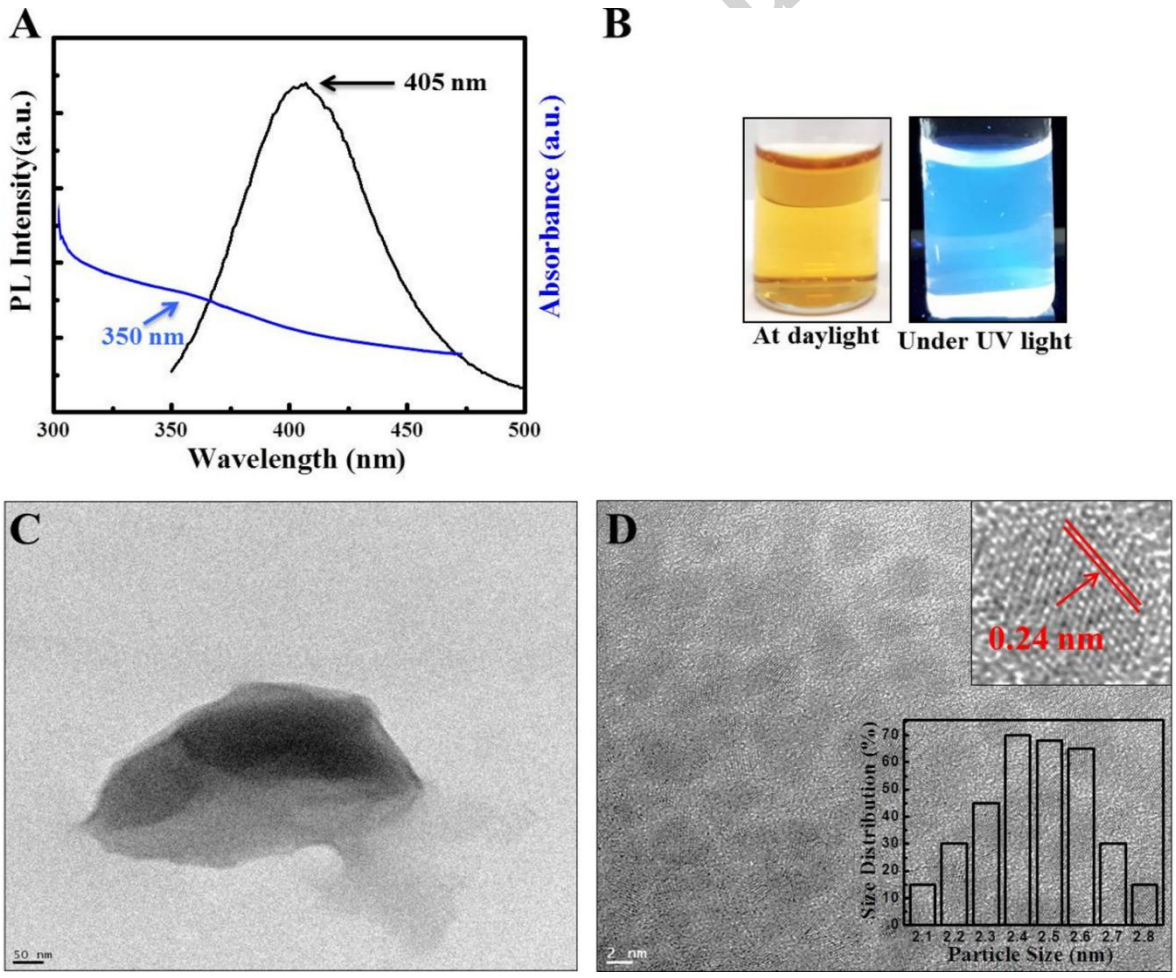

Figure 3: Spectroscopic and microscopic study of GQDs: (A) Fluorescence and absorbance spectra of GQDs; (B) Images of GQD solution under daylight and UV light; (C) TEM image of pristine graphene & (D) HRTEM image of synthesized GQDs (Inset: Particle size distribution profile & lattice pattern in GQD nanocrystals).

High-resolution transmission electron images (HRTEMs) of GQDs were acquired on an FEI Titan 8-300 TEM, equipped with a CEOS hexapole image corrector. The microscope was operated at 300 kV in bright-field TEM mode. We then dispersed 20 microliters of sample materials on a Ted Pella ultrathin carbon support film grid and air-dried. The sample was plasma-cleaned in a Gatan Solarus plasma cleaner using an Ne, H, Ar mixture for 30 seconds at 30W. As shown in Figure 3C, the length and diameter of the bulk graphene nanopowder was a few hundred nanometers. The HRTEM image of as-prepared GQDs demonstrated that QDs are well dispersed and uniform in size, with an average size of 2–3 nm (Fig. 3D). Such well-dispersed nanocrystals are considered advantageous for optical-based biosensor development, as they help to avoid aggregation and quenching issues. The closed HRTEM image confirmed that the prepared GQDs feature a highly paralleled and ordered lattice fringe structure and interlayer spacing of about 0.24 nm, as indicated by the (1120) lattice plane of the graphene (Fig. 3D).

The fluorescence decay dynamics of excited states of nanocrystals is significant in the understanding of its electro-optic and catalytic properties. Here, the fluorescence lifetime of GQDs was analyzed using Horiba Time-Resolved Fluorimeter (Model PPD-650, Ontario, Canada). The samples were excited at 336 nm using a Delta Diode laser, and the fluorescence intensity was measured as a function of time at the wavelength of maximum emission.

The fluorescence decays were then analyzed by fitting to a sum of exponentials according to the following Equation (2):

$$I(t) = I_o(t)\sum_i \alpha_i \exp\left[\frac{-t}{\tau_i}\right] \qquad (2)$$

In Equation (2) above, $I_o(t)$ represents the fluorescence intensity at t = 0, while □ and □ denote the pre-exponential factor and lifetime in time-bin i respectively. The lifetime decay profile of GQDs is shown in Figure 4A. The residuals and their autocorrelation were evenly distributed around zero (Figs. 4B and 4C). Three lifetimes were acquired for a good fit, characterized by χ^2 value (Fig. 4D). The average lifetime of the quantum dots was calculated according to Equation (3) below, and the calculated GQD lifetime equaled 1.57 ns.

$$< \tau >= \frac{\sum \alpha_i \tau_i}{\sum \alpha_i} \qquad (3)$$

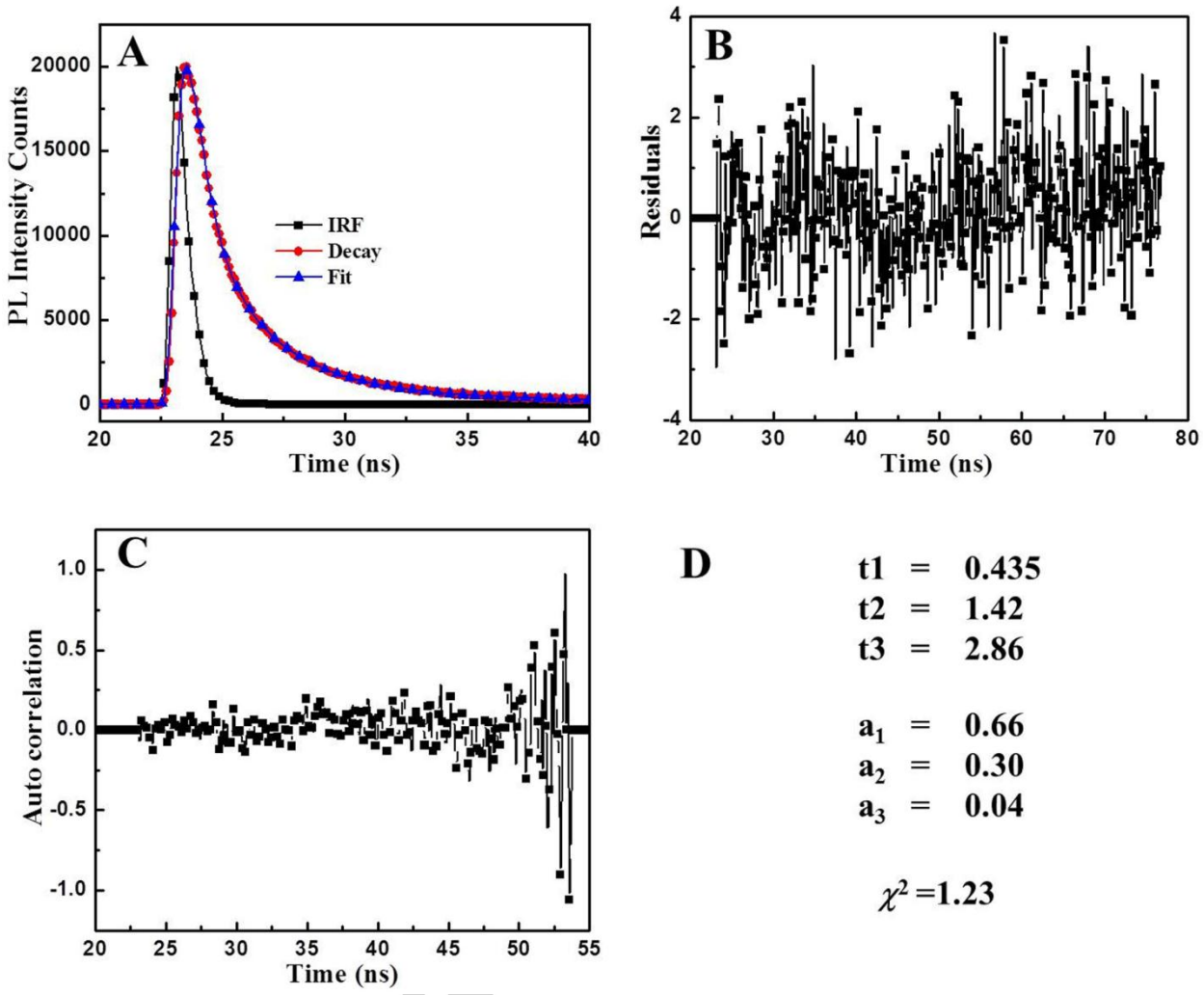

Figure 4: Fluorescence lifetime of GQDs$_2$: (A) Fluorescence decays profile of GQDs, where (■) instrument response function; (•) decay and (▲) Fit; (B) The residuals; (C) Autocorrelation of the residuals; and (D) Obtained three lifetimes and □^{2} value .

3.3 Confirmation of antibodies' specificity toward target virus

The specificity of anti-adenovirus antibodies for FAdVs was confirmed through the ELISA method. As shown in Figure S2, a higher optical density was achieved for anti-adenovirus antibodies in comparison to anti-H5N2 HA antibodies and BSA, illustrating the specificity of anti-adenovirus antibodies toward FADVs.

3.4 Binding confirmation of anti-adenovirus antibodies with Au NBs and GQDs

The ELISA method was performed for checking the binding of anti-adenovirus antibodies with Au NBs and GQDs. In Figure S3, a higher absorbance was obtained for anti-adenovirus antibodies, confirming the successful binding between antibodies and GQDs. A step-by-step variation in zeta potential measurements (Zetasizer Nano ZS, Malvern Instruments Ltd., Worcestershire, UK) also confirmed the successful conjugation of antibodies with GQDs (Table S1). The amide bond formed between anti-adenovirus antibodies and Au NBs was further confirmed by an FTIR spectrum. As shown in Fig. S4, FTIR bands found at 3500–3700 cm^{-1} and 1630–1690 cm^{-1} represent amide N–H stretching and amide C=O stretching respectively.

Furthermore, the Nyquist plots of electrochemical impedance spectroscopy (EIS) for different experimental conditions were investigated in this study. EIS were recorded in the presence of 5 mM $[Fe(CN)_6]^{3-/4-}$ as a redox probe in 1X PBS buffer using PalmSens4 potentiostat. EIS data were acquired across a frequency range of 1 Hz–100 KHz, with a fixed potential of 100 mV and an amplitude of 10 mV. The Nyquist plot was obtained after fitting the data using the Randles circuit. For the bare electrode, the plot is nearly a straight line, indicating a diffusion-limiting electrochemical process. When the electrode was coated with Au NB, the plot is smaller and a straight line, implying a drastic decrease in the resistance of electrode. After immobilizing the antibodies, the semicircle is observed to have a significant large diameter, suggesting the coating of Au NB with insulating protein layer. Finally, the interaction of antibodies with the target and GQDs regained the impedance. It further revealed that the presence of Au NB and GQDs enhanced the rate of electron transfer and diffusion was highly dominant (Fig. S5).

3.5 Optoelectronic Bioassay of FAdVs

Every step of the fabrication of the sensor electrodes before and after each treatments, and detection was confirmed and validated through SEM, ELISA method, FTIR spectrum and DLS measurements. After confirming the binding of antibodies with Au NBs and GQDs, an optoelectronic assay was performed based on the redox behavior of the Au NB–GQD nanohybrids in the ferro/ferri electrolyte. The results of the biosensor output are shown in Figure 5. A significant enhancement of peak current was observed for the Au NB–fabricated carbon electrode compared to a bare electrode due to the excellent electric properties of the Au nanostructure; the enhancement makes it a promising candidate for electric signal enhancement–based biosensor development. The peak current corresponding to the reduction of Fe^{3+} to Fe^{2+} for antibody-conjugated Au NBs was decreased compared to the Au NB–fabricated carbon electrode because of the passivation of the electrode surface by non-conductive antibodies that block the diffusion of the redox marker ions. However, with the addition of a GQD–Ab/FAdV complex to Ab–Au NBs, an immuno-assembly of Au NBs–GQDs was formed, and the electric signal was further enhanced due to the local electric field enhancement effects (Fig. 5A).

These results indicate that the fabricated electrode with Au NBs exhibited a good analytical performance that enables its applicability for sensitive bio-detection techniques. In this study, the enhancement of the electric signal was correlated with the addition of various concentrations of FAdVs. The change in electric current with different viral concentrations was carefully examined (Fig. 5B), and a calibration curve of current vs. FAdV concentration was constructed. The current response with different concentrations of virus was observed in the range of 10 PFU/mL to 10000 PFU/mL with an LOD value of 8.75 PFU/mL (Fig. 5C). Here, LOD value was

calculated based on standard deviation method i.e., 3 times the standard deviation of blank electric signal (n = 10) divided by slope of the regression equation:

$$\mathrm{LOD} = \frac{3.\mathrm{SD}}{\mathrm{m}}$$

where SD and m indicate the standard deviation of the mean blank signal and the slope of the linear regression curve, respectively.

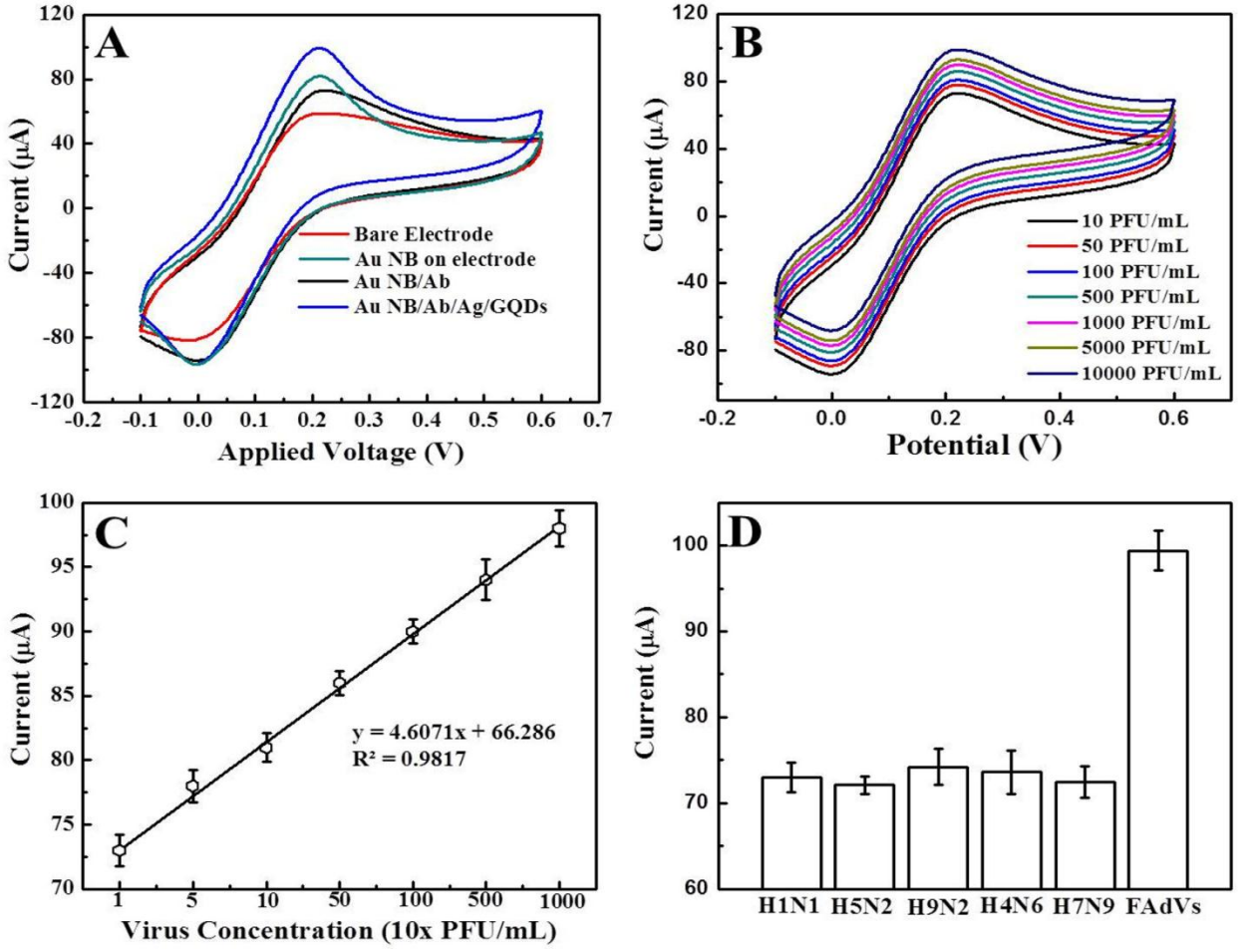

Figure 5: Optoelectronic nanobiosensor of FAdVs: (A) The CV curves at different stages of carbon electrode modification, recorded at a fixed scan rate of 50 mV s^{-1} in a redox probe solution of 10 mM $[Fe(CN)_6]^{3-}$ + 10 mM $[Fe(CN)_6]^{4-}$ prepared in 100 mM PBS buffer; (B) The responses of the current to different concentrations of FAdVs; (C) The calibration curve of current vs. virus concentration and (D) The selectivity results of FAdV detection.

The selectivity test of the proposed optoelectronic bioassay was implemented with other virus strains, namely H1N1 (1 µg/mL), H5N2 (1 µg/mL), H9N2 (100 HAU/50 µL), H4N6 (100 HAU/50 µL) and H7N9 (1 µg/mL); a significant enhancement in electric response was obtained with the target FAdVs (1000 PFU/mL) in comparison to the other strains, demonstrating that the proposed optoelectronic bioassay is selective only to the detection of target FAdVs (Fig. 5D). The sensitivity of the developed optoelectronic bioassay was validated with the conventional ELISA method (Table S2). The visual color response of the conventional ELISA method was up to 1000 PFU/mL, indicating that the optoelectronic-based bioassay is 100 times more sensitive than the conventional ELISA. In terms of final assay time responses, the proposed assay takes less than a minute while conventional ELISA method needs 30 min.

The real-life applicability of the proposed method was further investigated with a biological complex, i.e., chicken blood. The current response with different concentrations of virus in chicken blood was observed in the range of 50 PFU/mL to 10000 PFU/mL with an LOD value of 37.15 PFU/mL (Fig. S6), indicating the feasibility, sensitivity, and selectivity of proposed biosensor even in complex media (Fig. S7). All the experiments were performed in triplicate and repeated three times with similar results. Hence, the results presented were highly reproducible and repeatable. Constant sensor response was retained and no significant loss of signal was observed from the sensors stored under refrigerated conditions for over 60 days

4. Conclusions

In this work, shape-controlled and well-defined gold nanostructures have been fabricated on electrode as a sensing platform by using a simple and template-free *in situ* modified LbL method.

SEM was used to monitor the morphology regulation by changing the concentration of L-(+)-ascorbic acids. On the basis of surface morphology, Au NBs were selected as an optoelectronic sensing platform for highly sensitive and selective FAdV detection in buffer and blood samples due to its excellent optical confinement properties and easy preparation. The proposed sensor showed its detection ability up to 10 PFU/mL and 50 PFU/mL in buffer and blood media, respectively. The present results were validated with the conventional ELISA method, and the results revealed that the present study yielded a higher sensitivity than conventional ELISA methods. Due to the excellent sensing performance, Au NBs would be a potential component in detection platforms for other sensing techniques, such as electrochemistry-based sensing, metal-enhanced fluorescence-based sensing, surface plasma resonance or surface-enhanced Raman scattering techniques. In the meantime, the proposed optoelectronic sensing assay may become a new strategy for biological and chemical molecule detection.

Acknowledgements

The authors sincerely thank the Natural Sciences and Engineering Research Council of Canada (400705) for funding this study.

Appendix. Supporting information

Supplementary data associated with this article can be found in the online version at http://XXXX

References

Achermann, M., 2010. J. Phys. Chem. Lett. 1, 2837–2843.

Ahmed, S. R., Cha, H. R., Park, J. Y., Park, E. Y., Lee, D., and Lee, J., 2012. Nanoscale Res Lett. 7, 438.

Ahmed, S. R., Hossain, M. A., Park, J. Y., Kim, S., Lee, D., Suzuki, T., Lee, J., Park, E. Y., 2014. Biosens. Bioelectron. 58, 33–39.

Ahmed, S. R., Takemeura, K., Li, T., Kitamoto, N., Tanaka, T., Suzuki, T., Park, E. Y., 2017. Biosens. Bioelectron. 87, 558–565.

Alexander, H. S., Huber, P., Cao, J., Krell, P. J., Nagy, É., 1998. J. Virol. Methods 74, 9–14.

Ariga, K., Hill, J. P., Ji, Q., 2007. Phys. Chem. Chem. Phys. 9, 2319–2340.

Bansal, A. K., Hou, S., Kulyk, O., Bowman, E. M., Samuel, I. D. W., 2014. Adv. Mater. 27, 7638–7644.

Cohen-Hoshen, E., Bryant, G. W., Pinkas, I., Sperling, J., Bar-Joseph, I., 2012. Nano Lett. 12, 4260–4426.

Hanke, T., Cesar, J., Knittel, V., Trügler, A., Hohenester, U., Leitenstorfer, A., Bratschitsch, R., 2012. Nano Lett. 12, 992–996.

Jiang, R., Li, B., Fang, C., Wang, J., 2014. Adv. Mater. 26, 5274–5309.

Kauranen, M., Zayats, A. V., 2012. Nat. Photonics 6,737–748.

Lee, J., Hernandez, P., Lee, J., Govorov, A. O., Kotov, N. A., 2007. Nat. Mater. 6, 291–295.

Lu, W., Lieber, C. M., 2007. Nat. Mater. 6, 841–850.

Mittal, D., Jindal, N., Tiwari, A. K., Khokhar, R. S., 2014. Virus Dis. 25, 114–119.

Oh, E., Liu, R., Nel, A., Gemill, K. B., Bilal, M., Cohen, Y., Medintz, I. L., 2016. Nat. Nanotechnol. 11, 479–486.

Oulton, R. F., Bartal, G., Pile, D. F. P., Zhang, X., 2008. New J. Phys. 10, 105018.

Ojkíc, D., Krell, P. J., Tuboly, T., Nagy, É., 2008. Can. J. Vet. Res. 72, 236–241.

Saha, K., Agasti, S. S., Kim, C., Li, X., Rotello, V. M., Chem. Rev. 2012. *112*, 2739–2779.

Schuller, J. A., Barnard, E. S., Cai, W., Jun, Y. C., Justin S. White, J. S., Brongersma, M. L., 2010. Nat. Mater. 9,193–204.

Sun, H., Wu, L., Wei, W., Qu, X., 2013. Mater. Today 16, 433–442.

Soenen, S. J., Manshian, B. B., Aubert, T., Himmelreich, U., Demeester, J., Smedt, S. C. D., Hens, Z., Braeckmans, K., Chem. Res. Toxicol. 2014, 27, 1050–1059.

Tan, S. J., Campolongo, M. J., Luo, D., Cheng, W., 2011. Nat. Nanotechnol. 6, 268–276.

Thiruvengadathan, R., Korampally, V., Ghosh, A., Chanda, N., Gangopadhyay, K., Gangopadhyay, S., 2013. Rep. Prog. Phys. 76, 066501.

Todisco, F., D'Agostino, S., Esposito, M., Fernández-Domínguez, A. I., Giorgi, M. D., Ballarini, D., Dominici, L., Tarantini, I., Cuscuná, M., Sala, F. D., Gigli, G., Sanvitto, D., 2015. ACS Nano 9, 9691–9699.

Wang, D., Chen, J., Dai, L., 2015. Part. Part. Syst. Charact. 32, 515–523.

Yang, A., Wang, D., Wang, W., Teri W. Odom, T. W., 2017. Annu. Rev. Phys. Chem. 68, 83–99.

Yu, H., Regulacio, M. D., Ye, E., Han, M., 2013. Chem. Soc. Rev. 42, 6006–6018.

Zhang, Q., Lee, L., Joo, J. B., Zaera, F., Yin, Y., 2013. Acc. Chem. Res. 46, 1816–1824.

Zheng, P., Wu, N., 2017. Chem. Asian J. 12, 2343–2353.

Zhou, S., Xu, H., Gan, W., Yuan, Q., 2016. RSC Adv. 6, 110775.

Highlights

- Optoelectronic biosensor to detect Fowl Adenovirus was developed.
- The developed biosensors was based on gold nanobundles-graphene quantum dots hybrids.
- Assay had a detection limit of 8.75 PFU/mL with linear range from 10 to 10000 PFU/mL.
- Proposed sensing strategy was 100 times more sensitive than conventional ELISA method.
- Present bioassay may become a new strategy for biological and chemical molecules detection.